Master of Science in Mechanical Engineering

Quasi-Static Analysis of an Electrohydraulic Actuator for a Soft Gripper

소프트 그리퍼를 위한 전기 유압 액츄에이터의 준정적 해석

February 2023

Graduate School of Mechanical Engineering
Seoul National University

이 강 현

Quasi-Static Analysis of an Electrohydraulic Actuator for a Soft Gripper

Advisor 김 찬 중

Submitting a master's thesis of
Mechanical Engineering

October 2022

Graduate School of Mechanical Engineering
Seoul National University

이 강 현

Confirming the master's thesis written by
이 강 현

December 2022

Chair	박희재	(Signature)
Vice Chair	김찬중	(Signature)
Examiner	차영수	(Signature)

Abstract

In this study, we develop an analytical model for an electrohydraulic actuator operating with polyethylene pouches, polydimethylsiloxane backbone plates, and dielectric fluids, to analyze its performance considering the displacement. We assume a soft gripper based on two facing electrohydraulic actuators and theoretically estimate the gripper performance in two respects: the workspace and the grasping force. Finally, we conduct parametric studies by varying three parameters: the length of backbone plate, the amount of dielectric fluid, and the permittivity of the dielectric fluid, to demonstrate the changes in performance according to their values.

Keyword : Electrohydraulic force, Electrostatic force, Soft gripper, Quasi-static analysis, Energy analysis, Solid mechanics, Beam analysis
Student Number : 2021-29356

Table of Contents

Chapter 1. Introduction

Most machines and robots are made of hard materials, such as metal and plastic. Hard robots have performed a major role in the evolution of modern civilization [1, 2, 3]. Recently, as industries have gradually diversified, the limitations of hard robots have begun to emerge. Owing to the lack of hard material flexibility and softness, their designs tend to be limited by the ambient environment, and the types of objects handled are restricted [4, 5, 6, 7, 8].

In this context, different robot types are required to delicately treat fragile substances. For this reason, soft robots have recently received considerable attention as a solution for this type of task [9, 10, 11]. Soft robots have advantages in handling deformable, brittle, and irregularly shaped objects with their soft elements. They can flexibly interact with the surroundings and humans, and are increasingly being applied to various fields, including biomimetic technology and wearable devices [12, 13, 14, 15, 16, 17, 18].

A hydraulically amplified self-healing electrostatic (HASEL) actuator, which is a type of soft actuator, is operated by electrostatic power and an inner working fluid [19, 20, 21, 22, 23]. A HASEL actuator is based on the Peano actuator, which uses soft materials as its body and a dielectric fluid as its working fluid [24]. Several types of soft robots have been developed using HASEL

actuators. Acome et al. developed a flat cylindrical HASEL actuator with electrodes attached at the center of the top and bottom faces of the cylindrical-shaped actuator.[20]. As the two electrodes approach each other by electrostatic force, the liquid dielectric is pushed to the edge of the cylindrical shell, and the edge swells up, generating force; however, this actuator moves and generates force in only one direction. The research group also proposed a soft gripper using two multilayered actuators; however, owing to the large default volume of the cylindrical shape, the grasping motion range is limited. Kellaris et al. reported a muscle-mimetic system with HASEL actuators consisting of arranged flexible and extensible shells [19]. They implemented muscle relaxation and contraction by allowing a liquid dielectric to enter and exit the shells via electrostatic force. Although it generates force like a muscle, its range of motion is one-dimensional and it works only in the gravitational direction because there are no rigid links between the arranged shells. Another study by this group developed a mechanical joint that realizes a bendable HASEL actuator [25]. A gripper system with three flat two-joint fingers was designed using this joint. The system has six electrodes, two on each side of the three fingers, such that it can control each joint of the gripper' s finger in both directions. In addition, the grasping torque is higher than that of general servo motor. Despite these advantages, because most of the fingers, except the joints, are made of hard materials including rigid stiffeners, they may damage soft and fragile objects while grasping them. Furthermore, because the

electrodes are located at the finger touching side, there is a high risk of damage to the electrodes.

For a higher level of understanding and sustainable development of HASEL actuators and soft grippers, both actual experiments and sufficient theoretical analysis are important. There are several studies on actuation system modeling [23, 26, 27, 28, 29], and theoretical analysis of these hydraulic soft actuators are also conducted [27, 28, 30, 31, 32]. Various methods such as statics, dynamics, and reduced order modeling are established to verify and predict the performance of actuators. The theoretical verification process is essential because it demonstrates the efficiency of the newly developed actuator structure and helps to find an optimized design.

A recent study by our group proposed an electrohydraulic actuator used as a soft gripper, as depicted in Fig. 1 [33]. It consists of three polyethylene (PE) film pouches, two electrodes, and dielectric fluid.

Two facing electrodes are connected to a voltage source, and a dielectric fluid exists between them. The dielectric fluid is Mictrans A, which is based on uninhibited mineral oil. A series of three pouches are connected to the electrodes. There are fine gaps between the pouches that act as both passageways through which the dielectric fluid passes and hinges between the pouches. A thick but bendable silicone backbone plate, which distinguishes our actuator from other HASEL actuators, is attached to one side of the actuator. Thus, the actuator can easily bend in a certain direction

and can be applied to a soft gripper as a robotic finger.

In this study, we introduce a theoretical modeling framework for an electrohydraulic actuator with a backbone plate and soft gripper. Additionally, we conduct the analysis in terms of three key aspects: deriving the vertical displacement, the workspace volume, and the grasping force. Specifically, we obtain the theoretical values of the actuator vertical displacement from the model and compare them with the experimental values [33] to validate the model. We then estimate the workspace volume and the grasping force based on the soft gripper design with two actuators. An alpha shape [34, 35, 36, 37] is introduced to calculate the workspace volume. Finally, we investigate how the three key actuator performance aspects change according to three parameters: the length of backbone plate, the amount of dielectric fluid, and the dielectric fluid permittivity.

Chapter 2. Theoretical model of an electrohydraulic actuator

2.1. Model establishment

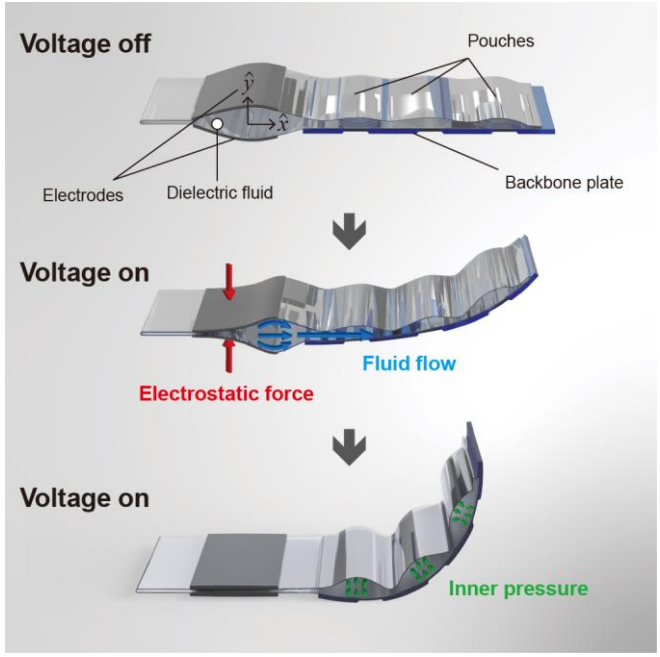

Figure 1: Fundamental principle of operation of an electrohydraulic actuator with a backbone plate.

When a voltage is applied to the two electrodes, the electrodes are attracted to each other owing to the electrostatic force. Accordingly, the dielectric fluid between the electrodes moves toward the pouches. As the pouches swell, the entire system bends in one direction by the strain of the silicone backbone plate. Fig. 1 shows the basic principle of the actuator operation [33].

The pouches of the electrohydraulic actuator swells because the dielectric liquid forms the pressure while the ends of each side are fixed to each other. We modeled lower side of the swollen shape, which consists of polydimethylsiloxane (PDMS) backbone plate, as a cantilever beam in two-dimensional coordinates x and y, as shown in Fig. 2. The beam has a length of $3L$ and a width of D, as

same as the backbone plate. P is the pressure from the dielectric liquid. If only downward pressure is applied to the beam, it bends downward. However, because the actuator bends upward, we set the normal force F, which is the normal force applied to the boundaries of the pouches.

In order to analyze the behavior of the actuator, the quasi-static method was used. The proposed system operates in one degree-of-freedom. Therefore, focusing on only initial and final instantaneous states assuming them to be static states was considered as the simple method to effectively predict the performance of the actuator. In other words, the hydrodynamic force due to the flow of the dielectric fluid was not considered in this study. The following assumptions were made to calculate the vertical displacement of the electrohydraulic actuator with the cantilever beam model.

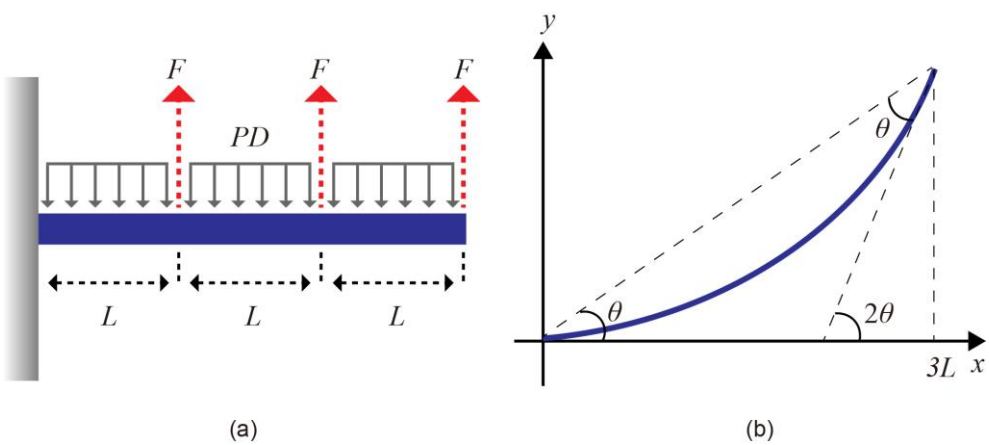

Figure 2: Cantilever beam model with kinematic parameters of a swollen pouch.

1. The connection between the electrodes and the nearest pouch is firmly fixed so that the slope at the point remains constant at zero.
2. Three pouches contain same amount of dielectric liquid so that the effects from the liquid including pressure and strain are the same.
3. The strain energy of PE film is negligibly small compared to that of PDMS.
4. Both ends of the backbone plate bend at the same angle.
5. PDMS backbone plate behaves linearly elastically.
6. The whole system is uniform in the direction of width so that the plane stress/strain equations can be used.
7. The deformation angle and displacement of actuator are small enough comparing to the whole length of the actuator.

The connection between the electrodes and the nearest pouch is almost straight without curve. In order to establish fixed-free end beam, this connection is assumed to be firmly fixed. The second and fourth assumption are presented to make the beam model simple and easy to calculate without various unknowns. Additionally, the effect from the dielectric fluid is difficult to generalize depending on the actuating position due to the unspecificity of liquid behavior in the direction of gravity. This is another reason why those two assumptions are established. The PE film is very thin compared to the PDMS backbone plate and does not elastically deform. Therefore, it is assumed to be neglected in the energy equation. The backbone plate is assumed to have linear

elasticity to make the simple and easy model and to predict the performance of the actuator. Finally, the sixth and seventh assumptions are fundamental conditions for using 2−D cantilever beam theory.

Accordingly, the vertical displacement of the beam, which is the y−axis coordinate value of the beam, can be obtained with following equation:

$$\begin{cases} y(x) = -\dfrac{PD}{24EI}x^4 + \dfrac{PDL-F}{2EI}x^3 - \dfrac{9PDL^2-12FL}{4EI}x^2 & (0 \le x \le L) \\ y(x) = -\dfrac{PD}{24EI}x^4 + \dfrac{3PDL-2F}{6EI}x^3 - \dfrac{9PDL^2-10FL}{4EI}x^2 + \dfrac{FL^2}{2EI}x - \dfrac{FL^3}{6EI} & (L \le x \le 2L) \\ y(x) = -\dfrac{PD}{24EI}x^4 + \dfrac{3PDL-F}{6EI}x^3 - \dfrac{9PDL^2-6FL}{4EI}x^2 + \dfrac{5FL^2}{2EI}x - \dfrac{3FL^3}{2EI} & (2L \le x \le 3L) \end{cases} \quad (1)$$

where E is the Young' s modulus of PDMS, and I is the area moment of inertia of PDMS.

The slope of the beam can also be calculated by differentiating Eq. 1.

$$\begin{cases} \dfrac{dy}{dx}(x) = -\dfrac{PD}{6EI}x^3 + \dfrac{3PDL-3F}{2EI}x^2 - \dfrac{9PDL^2-12FL}{2EI}x & (0 \le x \le L) \\ \dfrac{dy}{dx}(x) = -\dfrac{PD}{6EI}x^3 + \dfrac{3PDL-2F}{2EI}x^2 - \dfrac{9PDL^2-10FL}{2EI}x + \dfrac{FL^2}{2EI} & (L \le x \le 2L) \\ \dfrac{dy}{dx}(x) = -\dfrac{PD}{6EI}x^3 + \dfrac{3PDL-F}{2EI}x^2 - \dfrac{9PDL^2-6FL}{2EI}x + \dfrac{5FL^2}{2EI} & (2L \le x \le 3L) \end{cases} \quad (2)$$

We assume that both ends of the backbone plate bend at the same angle.

Then, following equations are derived using Eq. 1 and 2.

$$\tan\theta = \frac{y(3L)}{3L} = -\frac{27PDL^3}{8EI} + \frac{5FL^2}{EI} \quad \text{(3a)}$$

$$\tan 2\theta = \frac{dy}{dx}(3L) = -\frac{9PDL^3}{2EI} + \frac{7FL^2}{EI} \quad \text{(3b)}$$

$$F = \frac{EI\tan\theta}{5L^2} + \frac{27}{40}PDL = \frac{EI\tan 2\theta}{7L^2} + \frac{9}{14}PDL \quad \text{(3c)}$$

$$P = \frac{8EI}{9DL^3}(5\tan 2\theta - 7\tan\theta\ ) \quad \text{(3d)}$$

where θ is the bending angle at the end of the beam.

The bending moment is given by

$$M(x) = EI\frac{d^2y}{dx^2} \quad \text{(4a)}$$

$$\begin{cases} M(x) = -\dfrac{PD}{2}x^2 + (3PDL - 3F)x + 6FL - \dfrac{9}{2}PDL^2 & (0 \le x \le L) \\ M(x) = -\dfrac{PD}{2}x^2 + (3PDL - 2F)x + 5FL - \dfrac{9}{2}PDL^2 & (L \le x \le 2L) \\ M(x) = -\dfrac{PD}{2}x^2 + (3PDL - F)x + 3FL - \dfrac{9}{2}PDL^2 & (2L \le x \le 3L) \end{cases} \quad \text{(4b)}$$

With the bending moment M, the strain energy at the backbone plate of one pouch is given by

$$U_{strain} = \int_0^{3L} \frac{M(x)^2}{2EI}dx = \int_0^{L} \frac{M(x)^2}{2EI}dx + \int_L^{2L} \frac{M(x)^2}{2EI}dx + \int_{2L}^{3L} \frac{M(x)^2}{2EI}dx \quad (5)$$

The pressure energy of the dielectric liquid and the strain

energy of the backbone plate is generated from the electric energy of the electrodes, and the energy equation is given by

$$U_{electric} = U_{pressure} + U_{strain} \quad (6)$$

and each energy is expressed as follows:

$$U_{electric} = \frac{1}{2} C \overline{V}^2 \quad (7a)$$

$$U_{pressure} = PV_p \quad (7b)$$

$$U_{strain} = \frac{L^3}{EI}\left(\frac{243}{40} P^2 D^2 L^2 - \frac{211}{12} PDFL + \frac{77}{6} F^2\right) \quad (7c)$$

where C is the dielectric fluid capacitance and V is the input voltage. V_p is set to be $0.5 \times V_c$, which is the maximum fluid volume that three pouches can hold. V_c is set to be net volume of the three pouches when they swell to a maximum and form a cylinder. By reorganizing with $\overline{V}$, it is written as

$$\overline{V} = \sqrt{\frac{2}{C}(U_{pressure} + U_{strain})} \quad \left(C = \epsilon \frac{A}{d}\right) \quad (8)$$

where ϵ is the permittivity of the dielectric fluid, A is the size of the electrode, and d is the initial distance between the two electrodes.

In addition, the following formula for the end point displacement, y_d is applicable:

$$y_d = y(3L) = -\frac{81PDL^4}{8EI} + \frac{15FL^3}{EI} \quad (9)$$

With these equations, the relation between the input voltage and the displacement is established; the displacement of the actuator can be obtained from the input voltage. The input voltage range in this study is from 0kV to 12kV.

The real actuating mechanism is opposite to this derivation process. When the input voltage is applied to the electrodes, the dielectric fluid moves into the pouches and generates inner pressure. The swelling upper PE film pulls the connection points to the backbone plate which is presented as the normal force F in the derivation process. The generated pressure and force make the backbone plate bend so that the vertical displacement occurs which can be calculated with the displacement equations. As a result, the input voltage and the output displacement can be related both mathematically and physically.

The physical and geometric parameters used for the equations are listed in Table 1.

Table 1: Physical and geometric parameters of an electrohydraulic actuator [38, 33, 39, 40]. ϵ_0 is the dielectric constant, which is 8.854×10^{-12} F/m.

Parameters	Values

ϵ/ϵ_0	2.4
Vp/Vc	0.5
L	0.016m
D	0.04m
d	0.0043m
A	$0.0011\mathrm{m}^2$
V_c	$9.7785\times10^{-6}\,\mathrm{m}^3$
E	1.26MPa
I	$1.4063\times10^{-12}\,\mathrm{m}^4$

Fig. 3 shows the comparison between the theoretical and experimental data of y_d according to the input voltage. The displacement increases by the voltage increases in both experiment and theoretical estimation. In the whole section of voltage, the theoretical displacement is higher than the experimental value. Those two values have similar increasing tendency. However, there is a gap that cannot be ignored. The additional energy conversion is considered and the rise in potential energy is thought to be the reason. The experiment was conducted in a direction perpendicular to the bending direction of the actuator. Since the center of gravity moves in the opposite direction to gravity as the actuator bends, a part of the input electrical energy is converted to potential energy, as well as pressure and strain energy.

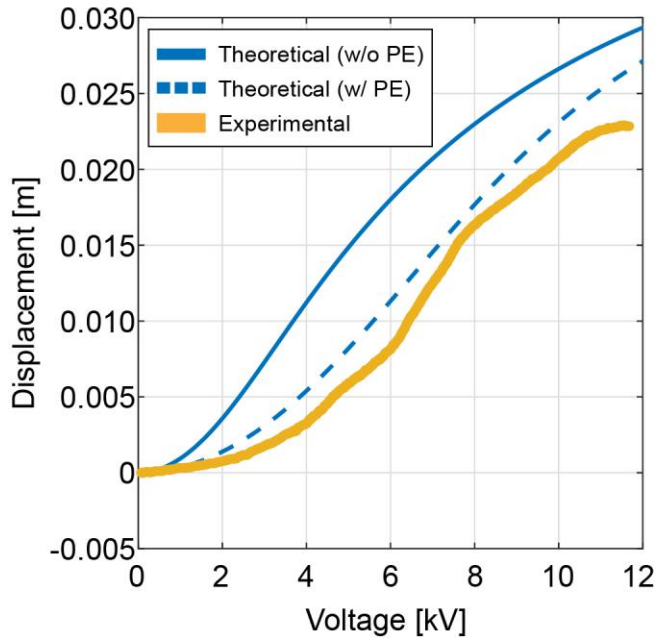

Figure 3: Theoretical and experimental relationship between the input voltage and y_d. The blue solid line is the theoretical value which does not reflect the potential energy (PE), and the blue dotted line is that reflecting the potential energy.

Therefore, the displacement reflecting the influence of gravity is newly calculated with following equations.

$$U'_{electric} = U_{pressure} + U_{strain} + U_{potential} \quad (10a)$$

$$U_{potential} = M_b g\left(\frac{1}{n}\Sigma_{k=1}^{n} y_k\right) \quad (10b)$$

where M_b is the mass of the backbone plate, which is 0.0014kg, g is the gravitational acceleration, and n is the arbitrary number of nodes. The nodes on backbone plate are assumed to be

$y(0)$, $y(L)$, $y(2L)$, and $y(3L)$. Therefore, n is 4. Accordingly, the potential energy is given by

$$U_{potential} = -\frac{M_b g L^3}{EI}\left(\frac{211}{48}PDL - \frac{77}{12}F\right) \quad (11)$$

The newly calculated displacement is plotted as the dotted blue line in Fig. 3. The increasing pattern appears similar to that of the experimental data.

As shown in Fig. 3, the maximum vertical deflection of the actuator is expected to be less than 0.03m while the whole length is 0.048m. Considering the relation between stress and strain of PDMS, the Young' s modulus remains almost constant during this level of deformation [41, 42, 43]. This result supports that the assumption of linear elasticity is reasonable.

Fig. 3 suggests that there is a correlation between the input voltage and the output displacement. In quasi-static aspect, the only input energy that system receives is the electrical energy and the only energy that changes within the system is pressure energy and deformation energy. This conversion of energy is due to the electrostatic attraction occurring between the electrodes, thereby the movement of the dielectric fluid. Additionally, the actuator is one degree-of-freedom system so that the mechanical output occurs only in one way. These factors enable the establishment of a function between the voltage and displacement, which means that those two can be derived from each other.

2.2. Physical meaning of the model

Understanding of the physical meaning of the theoretical model is important to relate the govern equations to the physical behavior principles of the system [44, 45, 46, 47, 48]. The start point of the model establishment is the derivation of the three beam equations: displacement, slope, and moment. The moment equations expressed as Eq. 4b can be derived with the force condition of the cantilever beam. The free body diagram (FBD) of the beam has to be considered first.

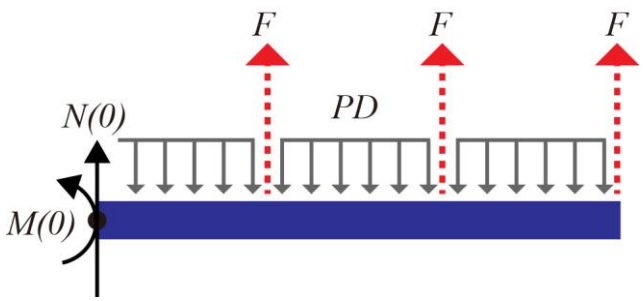

Figure 4: Free body diagram of cantilever beam model.

$N(0)$ and $M(0)$ is the normal force and torque on the left end point of the beam. In order for the beam to remain static, the values of both terms have to be calculated as follows:

$$N(0) = 3PDL - 3F \quad \text{(12a)}$$

$$M(0) = \frac{9}{2}PDL^2 - 6FL \quad \text{(12b)}$$

The next step is to divide the beam into three sections because three normal forces applied discontinuously. Therefore, the moment according to the point on the beam also has to be calculated separately as shown in Fig. 5.

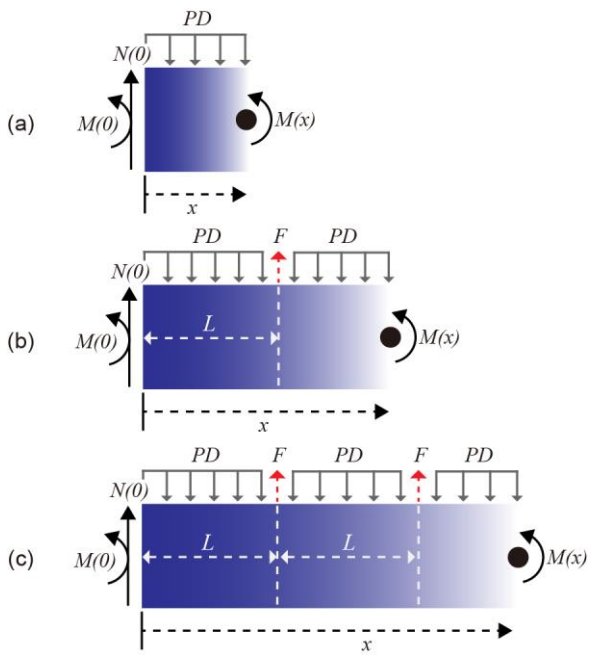

Figure 5: Free body diagrams of three sections: (a) $0 \leq x \leq L$, (b) $L \leq x \leq 2L$, and (c) $2L \leq x \leq 3L$

The distributed force is considered as one normal force applied in the middle point of the distributed range. The static equations of each section can be established as follows:

$$M(x) + M(0) - N(0)x + PDx(\frac{1}{2}x) = 0 \quad (0 \le x \le L) \tag{13a}$$

$$M(x) + M(0) - N(0)x + PDx(\frac{1}{2}x) - F(x-L) = 0 \quad (L \le x \le 2L) \tag{13b}$$

$$M(x) + M(0) - N(0)x + PDx(\frac{1}{2}x) - F(x-L) - F(x-2L) = 0 \quad (2L \le x \le 3L) \tag{13c}$$

The calculating results of these equations are the beam moment equations, Eq. 4b. The slope equations (Eq. 2) are obtained by integrating the moment equations, and the displacement equations (Eq. 1) are obtained by integrating them twice.

The moment of the beam is physically related to the energy that bent beam contains. The vertical displacement of the beam directly means the performance of the model. Therefore, it can be said that this cantilever beam model and its equations show how the performance of the actuator is generated from the energy of the system including electrical, pressure, and strain energy.

Except for energy equations, the bending mechanism of this model can be described in other aspects with various physical theories, for example, fluid mechanics and unit analysis.

When the electrodes are attracted to each other due to the electrostatic force, the zipping motion occurs from the end point of the electrodes as shown in the Fig. 1. Accordingly, the working fluid between the electrodes received force including the horizontal component which makes the fluid flows into the pouches. If all of the fluid moves into three pouches, it cannot go back into the

electrodes because they are attached to each other with the electrostatic force and there is no space between them. The working fluid trapped in the pouches forms pressure. Due to the pressure and coupled inner force on the connection points of the pouches, both upper and lower surface swell. The upper surface which is thinner has smaller radius than that of the lower surface. The material of the upper surface, PE film, loses its plasticity at the connection points in the fabrication process. On the contrary, the lower part consisting of the continuous PDMS backbone plate maintains its curvature at the connection points. As a result, the whole system bends according to the backbone plate curvature.

In general, the unit analysis is conducted as a basic method to physically verify a system. The initial form of the govern energy equation of the proposed model is the moment equation (Eq. 4b). The units of the right-hand side terms can be calculated as follows:

$$[kg \cdot m^{-1} \cdot s^{-2}][m][m]^2 + ([kg \cdot m^{-1} \cdot s^{-2}][m][m] + [kg \cdot m \cdot s^{-2}])[m] + [kg \cdot m \cdot s^{-2}][m] + [kg \cdot m^{-1} \cdot s^{-2}][m][m]^2 = [kg \cdot m^2 \cdot s^{-2}] \quad (14)$$

The simplified unit is as same as that of the moment. Therefore, the dimension of moment equation can be demonstrated.

Each term of the energy equation also has to be verified. The unit of energy terms presented in Eq. 7 can be calculated as follows:

$$[kg^{-1}\cdot m^{-2}\cdot s^{4}\cdot A^{2}][kg\cdot m^{2}\cdot s^{-3}\cdot A^{-1}]^{2}=[kg\cdot m^{2}\cdot s^{-2}\,] \quad (15a)$$

$$[kg\cdot m^{-1}\cdot s^{-2}][m^{3}]=[kg\cdot m^{2}\cdot s^{-2}\,] \quad (15b)$$

$$\frac{[m]^{3}}{[kg\cdot m^{-1}\cdot s^{-2}][m^{4}]}([kg\cdot m^{-1}\cdot s^{-2}]^{2}[m]^{2}[m]^{2}$$
$$+[kg\cdot m^{-1}\cdot s^{-2}][m][kg\cdot m\cdot s^{-2}][m]+[kg\cdot m\cdot s^{-2}]^{2})$$
$$=[kg\cdot m^{2}\cdot s^{-2}\,] \quad (15c)$$

All the units correspond to that of the energy and can be calculated with each other.

Lastly, the govern equations for the proposed system, Eq. 8 and Eq. 9 have to be analyzed in the aspect of unit. Each side of Eq. 8 can be presented as follows:

$$[kg\cdot m^{2}\cdot s^{-3}\cdot A^{-1}]=(\frac{[kg\cdot m^{2}\cdot s^{-2}]+[kg\cdot m^{2}\cdot s^{-2}]}{[kg^{-1}\cdot m^{-2}\cdot s^{4}\cdot A^{2}]})\frac{1}{2}$$
$$[kg\cdot m^{2}\cdot s^{-3}\cdot A^{-1}]=[kg\cdot m^{2}\cdot s^{-3}\cdot A^{-1}\,] \quad (16)$$

Units of Eq. 9 can be analyzed as follows:

$$[m]=\frac{[kg\cdot m^{-1}\cdot s^{-2}][m][m]^{4}}{[kg\cdot m^{-1}\cdot s^{-2}][m^{4}]}+\frac{[kg\cdot m\cdot s^{-2}][m]^{3}}{[kg\cdot m^{-1}\cdot s^{-2}][m^{4}]}$$
$$[m]=[m\,] \quad (17)$$

It can be verified that the unit of each side in both equations corresponds to each other.

Chapter 3. Results and discussion

3.1. Performance of a soft gripper based on electrohydraulic actuators

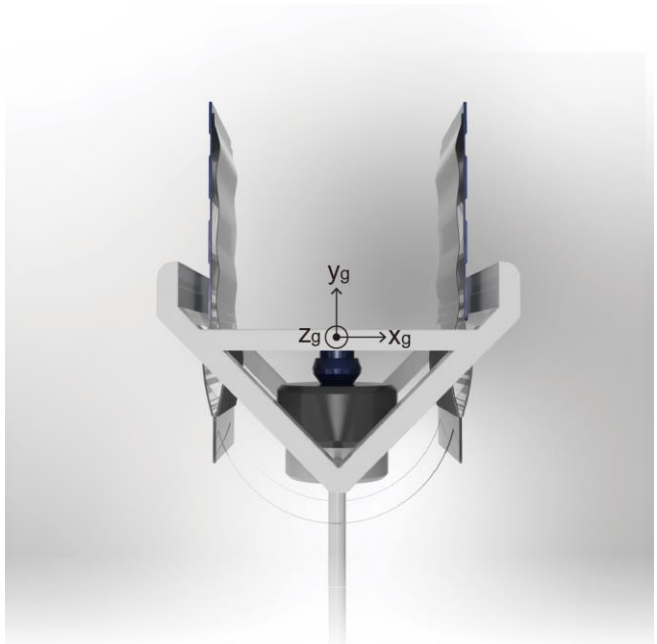

Figure 6: Schematic of the soft gripper.

Using the theoretical model, we study the performance of a soft gripper that consists of two facing actuators. Fig. 6 presents the concept design of the soft gripper [33]. In the soft gripper structure, the two actuators are designed to face each other with the side of the actuator is designed parallel to the ground. Thus, the theoretical model without the potential energy is chosen analyzing

the performance of the soft gripper.

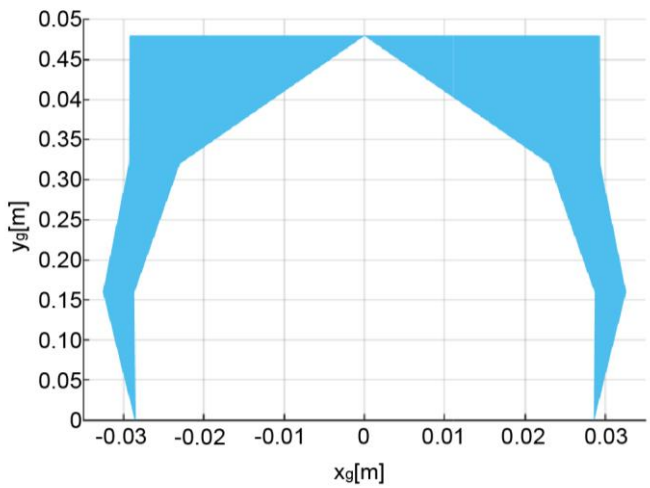

Figure 7: Top view of alpha shape for the soft gripper workspace.

Herein, we set the distance between the actuators as 0.06m, which is approximately twice the maximum value of y_d. To numerically quantify the workspace volume, an alpha shape is introduced, which is a group of linear simple curves that includes a finite number of points in the Euclidean plane. The alpha shape is useful for calculating the volume of an irregular shape changed by several parameters, containing a finite number of points. To visually verify the workspace and its change according to different parameter values, the alphaShape.m function of MATLAB (Matlab2019b, MathWorks, Inc.) was used.

The workspace alpha shape is shown in Fig. 7. The estimated workspace volume calculated as the alpha shape is $3.1650\times10^{-5}\mathrm{m}^3$. This volume contains only the node trajectories

and does not include the volume of the pouches. In the actual process, the pouches swell and become larger as the actuator bends. In other words, the actual workspace is larger than the estimated value. Moreover, considering that the working fluid volume is $9.7785 \times 10^{-6} m^3$, the gripper workspace is at least 3.2367 times the working fluid volume.

We also estimated the soft gripper grasping force by theoretically calculating the actuator bending moment with Eq. 4b. The maximum moment in the whole sections was considered as the grasping force of the gripper.

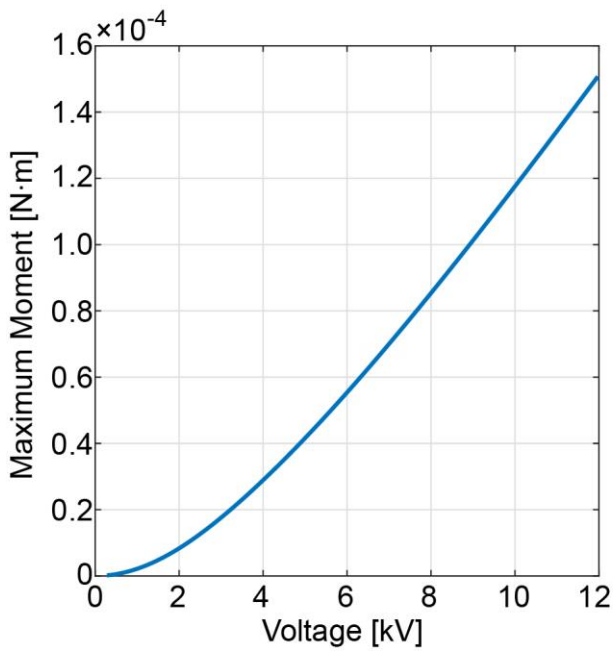

Figure 8: Maximum bending moment according to the input voltage.

Fig. 8 shows the change of maximum bending moment according to the input voltage. The maximum moment of the

actuator increases as the input voltage increases. The maximum moment increases up to 1.5071×10^{-4}N · m at 12kV.

3.2. Parameter study

To verify the changes in performance with changes in the actuator specification, three parameters were varied: the length of the backbone plate, the amount of dielectric fluid, and the dielectric fluid permittivity.

The length of the backbone plate is important when designing actuators. The length of actuator is directly related to the displacement and workspace. If a beam-shape actuator bends in a specific angle, the longer actuator has the larger displacement and workspace. However, the strain energy also differs according to the length of beam, it is required to be analyzed and estimated theoretically.

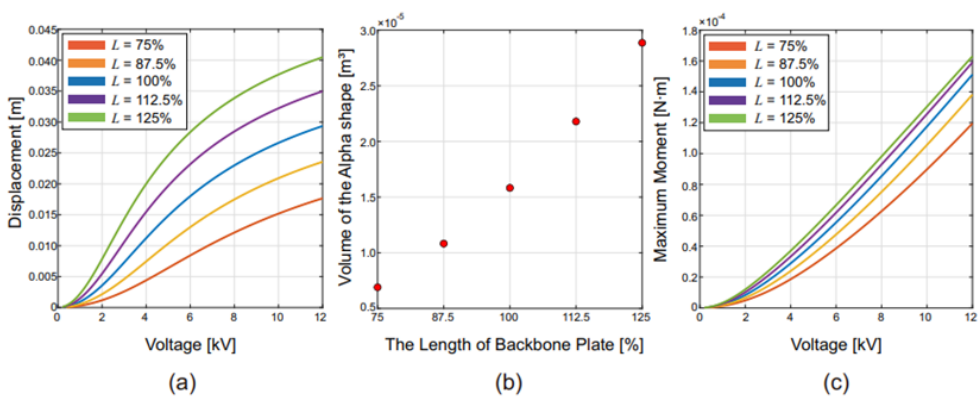

Figure 9: (a) Relationship between the input voltage and the displacement along with the length of the backbone plate. (b)

Volume of the alpha shape along with the backbone plate. (c) Relationship between the input voltage and the maximum moment along with the length of the backbone plate.

Fig. 9(a) shows how the displacement of an electrohydraulic actuator increases with voltage based on the length of the backbone plate. L is the length of one pouch so that the length of the backbone plate is $3L$. The initial value of L was 0.016m, which was used in the experiment, and we additionally calculated for the cases from 0.012m to 0.020m with intervals of 0.002m. For each voltage value, the longer actuator showed increased displacement while shorter one showed decreased.

The estimated workspace alpha shape volume according to the length is shown in Fig. 9(b). As the length of the actuator increased, the workspace of the two actuators in a soft gripper showed additional overlapping. For this reason, we calculated the workspace volume of only one actuator in this study. As shown in the graph, the workspace volume of one actuator increases as the length increases. The workspace volumes for L = 0.012m, 0.014m, 0.016m, 0.018m, and 0.020m were $0.6902\times10^{-5}\mathrm{m}^3$, $1.0828\times10^{-5}\mathrm{m}^3$, $1.5826\times10^{-5}\mathrm{m}^3$, $2.1793\times10^{-5}\mathrm{m}^3$, and $2.8858\times10^{-5}\mathrm{m}^3$, respectively. On average, as the length of the backbone plate increased by 0.006m, the volume increased by $0.5489\times10^{-5}\mathrm{m}^3$.

Fig. 9(c) shows the change of the maximum bending moment of the actuator according to the input voltage along with the length

of backbone plate. The increase in the maximum moment increases as the backbone plate becomes longer. In addition, the gap of moment at same voltage between each case decreases as the length increases.

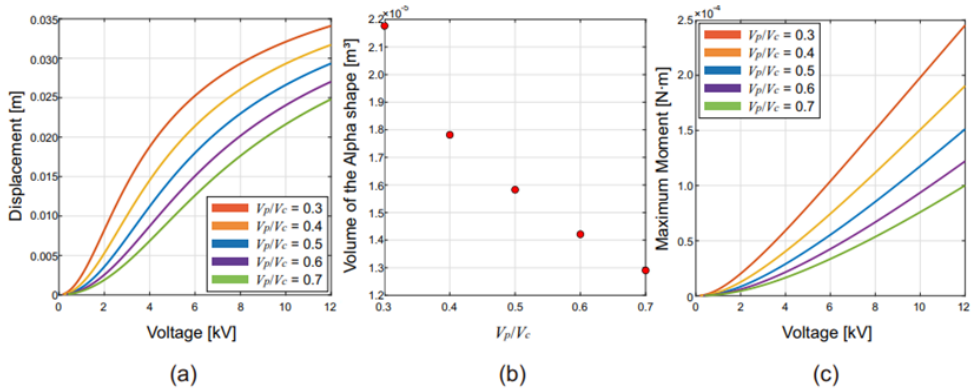

Figure 10: (a) Relationship between the input voltage and the displacement along with the amount of dielectric fluid. (b) Volume of the alpha shape along with the amount of dielectric fluid. (c) Relationship between the input voltage and the maximum moment along with the amount of dielectric fluid.

The second parameter is the amount of dielectric fluid. Membranes or pouches in contact with liquids behave in various manners according to the material and behavioral properties of the fluid [49, 50, 51]. Thus, it is important to understand the properties of the inner fluid to study a system that contains a working fluid.

The maximum amount of fluid, which is the net volume of the three pouches, is fixed as V_c. We varied the ratio of V_p to V_c and calculated y_d, workspace volume, and maximum bending moment of the actuator. The results are shown in Fig. 10.

Fig. 10(a) shows how the actuator displacement changes with the amount of fluid. The ratios of the fluid amount to the maximum are considered from 0.3 to 0.7 with 0.1 intervals. As the amount of working fluid increases, the displacement of the actuator decreases. The maximum displacement decreases from 0.0341m at a ratio of 0.3 to 0.0247m at a ratio of 0.7.

Fig. 10(b) shows the relationship between the fluid amount and the workspace volume. As the maximum displacement decreases, the workspace of the gripper also decreases according to the amount of fluid. The workspace volume decreases by $0.2216\times10^{-5}m^3$ on average as the ratio increases by 0.1.

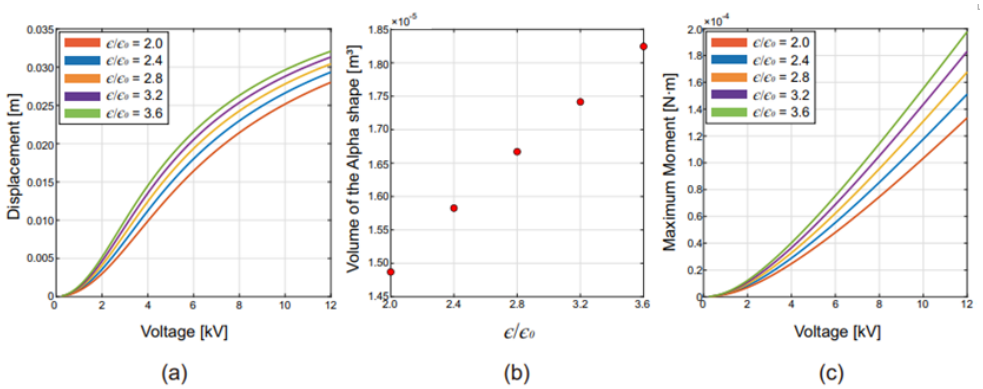

Figure 11: (a) Relationship between the input voltage and the displacement along with the relative dielectric fluid permittivity. (b) Volume of the alpha shape along with the relative dielectric fluid permittivity. (c) Relationship between the input voltage and the maximum moment along with the relative dielectric fluid permittivity.

Permittivity is an important material property of a fluid in an

electrical system. It is a factor that determines the capacitance, which is related to the electric energy [52, 53]. In the proposed system, the dielectric fluid was initially located between the two electrodes. The permittivity determines the inner pressure of the system by playing the roles of both the dielectric material and working fluid.

Fig. 11 shows how the actuator and soft gripper performance changes along with the relative dielectric fluid permittivity. The relative dielectric fluid permittivity is considered to be 2 to 3.6, which is the general range of permittivity for the mineral oil [38]. The displacement, workspace volume, and maximum moment increased as the permittivity increased. This is ascribed to the relationship between the permittivity and electric energy, which is the fundamental system input energy. The electric energy accommodated between the two electrodes is proportional to the capacitance, and the capacitance between the electrodes is proportional to the dielectric fluid permittivity. Therefore, all kinetic and kinematic changes based on the electric energy increase as the permittivity increases. In the case of the displacement, it increases by 0.0010m on average as the relative permittivity increases by 0.4. The workspace volume increases by $0.0843\times10^{-5}\mathrm{m}^3$ on average as the relative permittivity increases by 0.4. Finally, the maximum torque generated by the soft gripper increases by $0.1615\times10^{-4}\mathrm{N}\cdot\mathrm{m}$ on average as the permittivity increases by 0.4.

Chapter 4. Conclusion

In this study, we proposed an analytical model of an electrohydraulic actuator with a backbone plate and investigated a soft gripper based on it. Using the relationship between electrical energy, pressure energy, and strain energy in the system, we established several frameworks to estimate the performance in terms of the vertical displacement, workspace volume, and grasping force.

The estimated vertical displacement of the actuator was in good agreement with the experimental value. In addition, we studied a soft gripper based on two facing actuators. The volume of the alpha shape was calculated to quantify the soft gripper workspace.

Moreover, a parameter study was conducted by varying three parameters: the length of the backbone plate, the amount of dielectric fluid, and the dielectric fluid permittivity. We verified how the performance changed according to the variation in these parameters. The results indicated that all three performance aspects have a certain tendency with the parameters. Performances show positive relationship with the backbone plate length and the dielectric fluid permittivity while having negative relationship with the amount of dielectric fluid. This analysis result for the amount of dielectric fluid may seem counterintuitive because the fundamental actuating source in the proposed system is the amount of working fluid. However, this phenomenon can be explained in both physically

and geometrically. In the quasistatic aspect, the input electric energy at the initial state is converged to the pressure and strain energy at the final state. If the amount of fluid increases, the pressure energy also increases. Accordingly, in the same amount of the input energy, the part of the electrical energy which is converged to the pressure energy increases so that the strain energy decreases. In the geometric aspect, the connection points between the pouches become closer as the pouches swell during the operating mechanism. If the larger amount of fluid moves into the pouches and they swell more, the distance between points decreases which makes the total displacement also decrease. However, there are also factors that makes the bending displacement increase with larger amount of fluid. For example, the curvature of the beam model is occurred by the pressure from fluid. The curvature is directly related to the displacement so that larger pressure from the larger amount of fluid may increase the displacement. Therefore, analysis from more diverse aspects in this part has to be conducted in the future work.

Significant changes of the actuator performance depending on parameters mean that, negatively, the performance may be sensitive to damage caused by aging or external impacts. However, on the positive side, the optimal actuator for a variety of applications can be designed by adjusting the parameters appropriately. We derived improvements for future work from these analysis results. To develop a soft gripper that can grasp objects of various volumes with a high grasping force, it must be designed to

include enough lengths and a moderate amount of dielectric fluid with high permittivity.

The soft robotic system is difficult to analyze and design because of the unpredictable behavior due to the flexible and flowing materials. This quasistatic analysis using the beam model and energy equation was chosen as the useful method to simply and intuitively predict the performance of the electrohydraulic soft actuator. By establishing the method to calculate the displacement, workspace, and grasping force according to the input voltage and various parameters, the possibility to design various optimal soft grippers depending on usages was verified.

In real operating situation, there are other energy flows except for pressure and strain energy, and the constraints which are difficult to reflect the quasi-static method. Other methods for theoretical analysis will be considered for more rigorous verification of the model and better prediction of the performance in the future work. Considering other factors affecting the solid mechanics behavior of the beam model such as axial strain at different through-the-thickness locations and the effects of large displacements will also enable more accurate performance calculations.

Bibliography

[1] E. Appleton, D. J. Williams, Industrial robot applications, Springer Science & Business Media, 2012.

[2] J. Hudson, et al., The robot revolution, Books (2019).

[3] J. Wall´en, The history of the industrial robot, Linko¨ping University Electronic Press, 2008.

[4] C. Majidi, Soft robotics: a perspective—current trends and prospects for the future, Soft robotics 1 (2014) 5–11.

[5] S. Kim, C. Laschi, B. Trimmer, Soft robotics: a bioinspired evolution in robotics, Trends in biotechnology 31 (2013) 287–294.

[6] E. W. Hawkes, L. H. Blumenschein, J. D. Greer, A. M. Okamura, A soft robot that navigates its environment through growth, Science Robotics 2 (2017).

[7] D. Rus, M. T. Tolley, Design, fabrication and control of soft robots, Nature 521 (2015) 467–475.

[8] T. TolleyMichael, F. ShepherdRobert, C. GallowayKevin, J. WoodRobert, M. WhitesidesGeorge, et al., A resilient, untethered soft robot, Soft robotics (2014).

[9] M. Manti, T. Hassan, G. Passetti, N. D' Elia, C. Laschi, M. Cianchetti, A bioinspired soft robotic gripper for adaptable and effective grasping, Soft Robotics 2 (2015) 107–116.

[10] S. Mani, R. Perez, H. Lee, Z. Ounaies, W. Hung, H. Liang, Effects of applied potential on friction of a pvdf micro gripper, in: International Joint Tribology Conference, volume 42592, 2006, pp.

1145-1152.

[11] J. Shintake, V. Cacucciolo, D. Floreano, H. Shea, Soft robotic grippers, Advanced Materials 30 (2018) 1707035.

[12] Y.-Y. Xiao, Z.-C. Jiang, X. Tong, Y. Zhao, Biomimetic locomotion of electrically powered "janus" soft robots using a liquid crystal polymer, Advanced Materials 31 (2019) 1903452.

[13] K.-J. Cho, J.-S. Koh, S. Kim, W.-S. Chu, Y. Hong, S.-H. Ahn, Review of manufacturing processes for soft biomimetic robots, International Journal of Precision Engineering and Manufacturing 10 (2009) 171-181.

[14] C. Lee, M. Kim, Y. J. Kim, N. Hong, S. Ryu, H. J. Kim, S. Kim, Soft robot review, International Journal of Control, Automation and Systems 15 (2017) 3-15.

[15] M. Calisti, M. Giorelli, G. Levy, B. Mazzolai, B. Hochner, C. Laschi, P. Dario, An octopus-bioinspired solution to movement and manipulation for soft robots, Bioinspiration & biomimetics 6 (2011) 036002.

[16] Y. Nakabo, T. Mukai, K. Asaka, Biomimetic soft robots using ipmc, in: Electroactive Polymers for Robotic Applications, Springer, 2007, pp.
165-198.

[17] B. Shih, D. Shah, J. Li, T. G. Thuruthel, Y.-L. Park, F. Iida, Z. Bao, R. Kramer-Bottiglio, M. T. Tolley, Electronic skins and machine learning for intelligent soft robots, Science Robotics 5 (2020).

[18] J. Guo, C. Xiang, T. Helps, M. Taghavi, J. Rossiter,

Electroactive textile actuators for wearable and soft robots, in: 2018 IEEE International Conference on Soft Robotics (RoboSoft), IEEE, 2018, pp. 339–343.

[19] N. Kellaris, V. G. Venkata, G. M. Smith, S. K. Mitchell, C. Keplinger, Peano–hasel actuators: Muscle–mimetic, electrohydraulic transducers that linearly contract on activation, Science Robotics 3 (2018).

[20] E. Acome, S. Mitchell, T. Morrissey, M. Emmett, C. Benjamin, M. King, M. Radakovitz, C. Keplinger, Hydraulically amplified self–healing electrostatic actuators with muscle–like performance, Science 359 (2018) 61–65.

[21] S. K. Mitchell, X. Wang, E. Acome, T. Martin, K. Ly, N. Kellaris, V. G. Venkata, C. Keplinger, An easy–to–implement toolkit to create versatile and high–performance hasel actuators for untethered soft robots, Advanced Science 6 (2019) 1900178.

[22] P.–W. Lin, C.–H. Liu, Bio–inspired soft proboscis actuator driven by dielectric elastomer fluid transducers, Polymers 11 (2019) 142.

[23] P. Rothemund, S. Kirkman, C. Keplinger, Dynamics of electrohydraulic soft actuators, Proceedings of the National Academy of Sciences 117 (2020) 16207–16213.

[24] A. J. Veale, S. Q. Xie, I. A. Anderson, Characterizing the peano fluidic muscle and the effects of its geometry properties on its behavior, Smart Materials and Structures 25 (2016) 065013.

[25] N. Kellaris, P. Rothemund, Y. Zeng, S. K. Mitchell, G. M. Smith, K. Jayaram, C. Keplinger, Spider–inspired electrohydraulic

actuators for fast, soft-actuated joints, Advanced Science (2021) 2100916.

[26] P. Lochmatter, G. Kovacs, Design and characterization of an active hinge segment based on soft dielectric eaps, Sensors and Actuators A:
Physical 141 (2008) 577-587.

[27] N. Kellaris, V. G. Venkata, P. Rothemund, C. Keplinger, An analytical model for the design of peano-hasel actuators with drastically improved performance, Extreme Mechanics Letters 29 (2019) 100449.

[28] H. Wang, S. Cai, F. Carpi, Z. Suo, Computational model of hydrostatically coupled dielectric elastomer actuators, Journal of Applied Mechanics 79 (2012).

[29] S. Kirkman, P. Rothemund, E. Acome, C. Keplinger, Electromechanics of planar hasel actuators, Extreme Mechanics Letters 48 (2021) 101408.

[30] T. Hainsworth, I. Schmidt, V. Sundaram, G. L. Whiting, C. Keplinger, R. MacCurdy, Simulating electrohydraulic soft actuator assemblies via reduced order modeling, in: 2022 IEEE 5th International Conference on Soft Robotics (RoboSoft), IEEE, 2022, pp. 21-28.

[31] Q. Xie, T. Wang, S. Yao, Z. Zhu, N. Tan, S. Zhu, Design and modeling of a hydraulic soft actuator with three degrees of freedom, Smart Materials and Structures 29 (2020) 125017.

[32] K. Ly, J. V. Mayekar, S. Aguasvivas, C. Keplinger, M. E. Rentschler, N. Correll, Electro-hydraulic rolling soft wheel: Design,

hybrid dynamic modeling, and model predictive control, IEEE Transactions on Robotics (2022).

[33] T. Park, K. Kim, S.-R. Oh, Y. Cha, Electrohydraulic actuator for a soft gripper, Soft robotics 7 (2020) 68-75.

[34] L. Li, S. Rui, Q. Nie, X. Gong, F. Li, Conformal alpha shape-based multi-scale curvature estimation from point clouds., J. Comput. 7 (2012) 1460-1466.

[35] X. Jiang, S. Lou, P. J. Scott, Morphological method for surface metrology and dimensional metrology based on the alpha shape, Measurement science and technology 23 (2011) 015003.

[36] J. D. Gardiner, J. Behnsen, C. A. Brassey, Alpha shapes: determining 3d shape complexity across morphologically diverse structures, BMC Evolutionary Biology 18 (2018) 1-16.

[37] X. Xu, K. Harada, Automatic surface reconstruction with alpha-shape method, The visual computer 19 (2003) 431-443.

[38] T. Widyanugraha, P. Didit, et al., Dielectric properties of silicone oil, natural ester, and mineral oil under accelerated thermal aging, in: 2012 IEEE International Conference on Condition Monitoring and Diagnosis, IEEE, 2012, pp. 1139-1142.

[39] A. Peacock, Handbook of polyethylene: structures: properties, and applications, CRC press, 2000.

[40] C. Zhao, H. Qin, F. Gong, M. Feng, S. Zhang, M. Yang, Mechanical, thermal and flammability properties of polyethylene/clay nanocomposites, Polymer Degradation and Stability 87 (2005) 183-189.

[41] T. K. Kim, J. K. Kim, O. C. Jeong, Measurement of nonlinear

mechanical properties of pdms elastomer, Microelectronic Engineering 88 (2011) 1982–1985.

[42] R. Chang, Z. Chen, C. Yu, J. Song, An experimental study on stretchy and tough pdms/fabric composites, Journal of Applied Mechanics 86 (2019) 011012.

[43] K. Khanafer, A. Duprey, M. Schlicht, R. Berguer, Effects of strain rate, mixing ratio, and stress–strain definition on the mechanical behavior of the polydimethylsiloxane (pdms) material as related to its biological applications, Biomedical microdevices 11 (2009) 503–508.

[44] J. Wang, X. Guo, Adsorption isotherm models: Classification, physical meaning, application and solving method, Chemosphere 258 (2020) 127279.

[45] N. Sbirrazzuoli, Interpretation and physical meaning of kinetic parameters obtained from isoconversional kinetic analysis of polymers, Polymers 12 (2020) 1280.

[46] C. Fields, J. F. Glazebrook, A. Marciano, The physical meaning of the holographic principle, arXiv preprint arXiv:2210.16021 (2022).

[47] W. N. Plick, M. Krenn, Physical meaning of the radial index of laguerregauss beams, Physical Review A 92 (2015) 063841.

[48] J. W. Wagner, J. F. Dama, A. E. Durumeric, G. A. Voth, On the representability problem and the physical meaning of coarse–grained models, The Journal of Chemical Physics 145 (2016) 044108.

[49] A. Selvadurai, M. Shi, Fluid pressure loading of a

hyperelastic membrane, International Journal of Non-Linear Mechanics 47 (2012) 228- 239.

[50] M. Molki, K. Breuer, Oscillatory motions of a prestrained compliant membrane caused by fluid-membrane interaction, Journal of fluids and structures 26 (2010) 339-358.

[51] S. Das, K. F. Cheung, Coupled boundary element and finite element model for fluid-filled membrane in gravity waves, Engineering analysis with boundary elements 33 (2009) 802-814.

[52] S. Kondrat, A. Kornyshev, F. Stoeckli, T. Centeno, The effect of dielectric permittivity on the capacitance of nanoporous electrodes, Electrochemistry communications 34 (2013) 348-350.

[53] Q. Wang, L. Zhu, Polymer nanocomposites for electrical energy storage, Journal of Polymer Science Part B: Polymer Physics 49 (2011) 1421- 1429.

Abstract

본 연구는 폴리에틸렌 주머니, 폴리디메틸실록세인 백본 플레이트, 그리고 유전 액체로 작동하는 전기 유압 액츄에이터의 작동 변위에 대한 성능을 분석하기 위한 이론적 모델을 제시한다. 또한 두 개의 마주보는 전기 유압 액츄에이터로 구성된 소프트 그리퍼를 설계하고, 그 성능을 작동 범위와 파지 강도의 두 가지 측면에서 추정한다. 최종적으로, 백본 플레이트의 길이, 유전 액체의 양, 그리고 유전 액체의 유전율을 세 파라미터로 설정하고 이에 따른 그리퍼의 성능을 분석하는 파라미터 스터디를 수행하고 그 결과를 제시한다.